Realtime speckle sensing and suppression with project 1640 at Palomar

Gautam Vasisht, Eric Cady, Chengxing Zhai, Thomas Lockhart, Ben Oppenheimer

Gautam Vasisht, Eric Cady, Chengxing Zhai, Thomas Lockhart, Ben Oppenheimer, "Realtime speckle sensing and suppression with project 1640 at Palomar," Proc. SPIE 9148, Adaptive Optics Systems IV, 914822 (22 August 2014); doi: 10.1117/12.2056591

SPIE.

Event: SPIE Astronomical Telescopes + Instrumentation, 2014, Montréal, Quebec, Canada

Real-time Speckle Sensing and Suppression with Project 1640 at Palomar

Gautam Vasisht*[a], Eric Cady[a], Chengxing Zhai[a], Thomas Lockhart[a], Ben Oppeheimer[b] and the Project 1640 Collaboration

[a]Jet Propulsion Laboratory, California Institute of Technology, 4800 Oak Grove Drive, Pasadena, CA, USA 91109; [b]American Museum of Natural History, Central Park West at 79th, New York, NY, USA 10024.

ABSTRACT

Palomar's Project 1640 (P1640) is the first stellar coronagraph to regularly use active coronagraphic wavefront control (CWFC). For this it has a hierarchy of offset wavefront sensors (WFS), the most important of which is the higher-order WFS (called CAL), which tracks quasi-static modes between 2-35 cycles-per-aperture. The wavefront is measured in the coronagraph at 0.01 Hz rates, providing slope targets to the upstream Palm 3000 adaptive optics (AO) system. The CWFC handles all non-common path distortions up to the coronagraphic focal plane mask, but does not sense second order modes between the WFSs and the science integral field unit (IFU); these modes determine the system's current limit. We have two CWFC operating modes: (1) P-mode, where we only control phases, generating double-sided dark-holes by correcting to the largest controllable spatial frequencies, and (2) E-mode, where we can control amplitudes and phases, generating single-sided dark-holes in specified regions-of-interest. We describe the performance and limitations of both these modes, and discuss the improvements we are considering going forward.

Keywords: Exoplanets, coronagraphy, interferometry

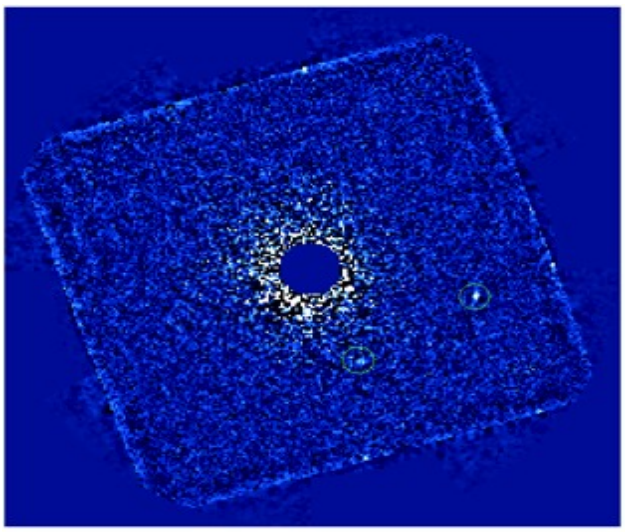

Figure 1: Speckle post-processed image of a survey target having twin candidate companions (within the demarcating circles). In raw images these candidates lie at the level of quasi-static and are not easily seen. In this example, a second observation with a ~1 yr baseline is needed to secure companionship. Precise spectra can be measured with a single E-mode observation.

1. INTRODUCTION

1.1 The Project

Project 1640, based at Palomar's 200-in telescope, was built to conduct a 99-night high contrast survey for planets, brown-dwarfs and debris disks orbiting nearby stars. It overcomes its site and aperture disadvantage (conditions at Palomar is not as good as Mauna Kea or some other Chilean sites) by use of technology, using the highest order AO system built for astronomy, anywhere, and supplementing it with active coronagraphic wavefront control. The latter capability offers some unique opportunities for innovating, that are, of course, more widely applicable in stellar coronagraphy.

The instrument (Oppenheimer et al. 2012; Hinkley et al. 2011) consists of a coronagraph and integral field spectrograph, the PALM 3000 Adaptive Optics system (Dekany et al. 2013) and the Wavefront Calibration System (Vasisht et al. 2014; Zhai et al. 2012; Cady et al. 2013), and is designed to search for and to characterize young, IR-luminous, Jovian-mass planets via low-resolution spectroscopy (R~35) and astrometry (~3 mas rms). All components of the end-to-end-system, including data extraction, reduction and speckle suppression software, are working well on the

Adaptive Optics Systems IV, edited by Enrico Marchetti, Laird M. Close, Jean-Pierre Véran, Proc. of SPIE Vol. 9148, 914822 · © 2014 SPIE
CCC code: 0277-786X/14/$18 · doi: 10.1117/12.2056591

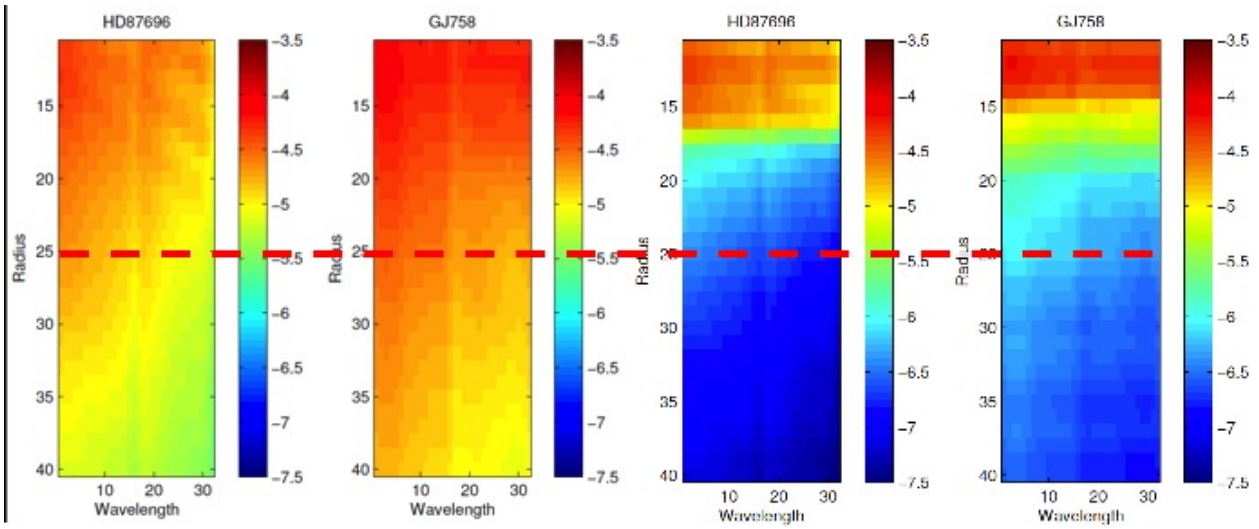

Figure 2: P-mode contrast maps for two stars before (left two panels) and after (right two panels) application of the post-processing S4 algorithm (Oppenheimer et al 2013; Fergus et al. 2014) which uses the full wavelength information in the data cube to improve the contrast by more than a factor of 10 to ~10^{-6} at 1" and as low as ~10^{-7} at 2.0". The IFS wavelength channels, J through H bands, are along the horizontal. The distance from the central star (in arbitrary units) is along the vertical, with the dashed red line at pixel 25 at 1". HD 87696 and GJ 758 (Thalmann et al. 2009) were observing in good and poor/moderate seeing conditions, respectively.

telescope, demonstrated by the first simultaneous imaging-spectroscopy of four planets orbiting a single star (HR 8799) in Oppenheimer et al. (2013) [Fig 4]. A forthcoming P1640 paper discussing astrometry/orbital motion of these four planets (Pueyo et al. 2014) draws interesting new conclusions about the inclination and eccentricity of the inner planets, and places the first observational constraints on the system's mean motion resonances. Overall we have published many refereed papers about the data acquired, and techniques developed, all of which, as well as further material, can be found at the website www.amnh.org/project1640. Our A-F star exoplanet survey was begun mid 2013.

Since the start of the Project 1640 survey we have observed ~30 target stars; of these stars, about 18 have been observed in good conditions, meaning clear nights with seeing better than 1.4" and with optimal wavefront control that results in post-processed threshold contrasts of 10^{-6} or $\Delta H = 15$ at 1" separation. For the subset of stars observed in good conditions, the detection efficiency for candidates is ~30 %. Confirmation of these candidates as gravitationally bound, however, must wait until a second "good-look" epoch after a sufficient time baseline has elapsed.

An example of a survey star with two candidates companions within P1640's small (3.8") field-of-view is in figure 1. During this first year of surveying, conditions have been relatively poor on the mountain with significant time lost to cloudy weather, ash-fall, or poor seeing from local weather patterns. However we expect to recover from this with the conditions returning to nominal averaged over the 3-yr survey period.

In the meantime we have taken advantage of the poor weather to make many improvements to the instrument, the data acquisition, and reducing observational overheads, carrying out many tests that are only possible with the instrument mounted to the telescope. With these improvements plus advances in post-processing speckle removal, we have been able to push our contrast limits to 10^{-6} at 1" even in conditions of mediocre seeing (figure 2). Spectroscopy of a faint T8.5 dwarf companion to the G8V star GJ 758 was acquired in such conditions (figure 2). It is also during this period that we have implemented the basic algorithm/code for instrument's "E-mode", designed to overcome the current raw-contrast floor, which is caused by wavefront amplitude distortions (further described in section 1.1.3).

1.2 The A-F Star Science Survey

Project 1640 is surveying mainly early type stars. Stars with spectral types between A0 and F5 offer a number of advantages for the coronagraphic survey. Most importantly, radial velocity (RV) and transit studies indicate that the incidence of giant planets increases in proportion to stellar mass with as many as 14% of A stars having a > 1 M_J

companion (< 5 AU) compared with only 2% of M stars (Johnson et al. 2010). Theoretical considerations preferentially favor A star hosts for the formation of giant planets on wide orbits via disk fragmentation (Dodson-Robinson et al. 2009). These theoretical and observational concepts appear to be borne out by the imaging of giant planets orbiting nearby A stars, e.g. HR 8799 (Marois et al. 2008, 2010) and β Pic (Lagrange et al. 2010) [also Kalas et al. 2008, Carson et al. 2013]. Finally, the intrinsic brightness of A and F stars makes them suitable for AO imaging while their youth (many < 1 Gyr) means that companions of a few Jupiter masses are bright enough for detection (Baraffe et al. 2003).

2. WAVEFRONT CONTROL

The incident stellar wavefront is a complex field, possessing both amplitude and phase imperfections over and above an ideal plane-wavefront. Both amplitude and phase accumulate distortions when propagating through the Earth's turbulent atmosphere and then through the imperfect telescope and instrument. AO coronagraphs seek to correct these distortions and suppress starlight as best as possible.

The turbulent atmosphere generates the large dynamic phase errors, as well as smaller scintillation error. AO systems measure and correct phase error (only), in real time, down to some fundamental limitations that can be classified as follows: Deformable mirror fitting error, wavefront sensor spatial aliasing, wavefront sensor measurement noise, and servo-lag error. Higher order AO systems, such as PALM 3000 and the GPI's AO (Macintosh et al 2014), surpass performance levels of ordinary AO systems by reducing the contribution of these four error terms down to ~ 80–120 nm rms. They do this by using higher order deformable mirrors correcting finer spatial scales, coupled to faster and more sensitive Shack-Hartmann (or other type) wavefront sensors. Amplitude error from scintillation is ignored by AO systems.

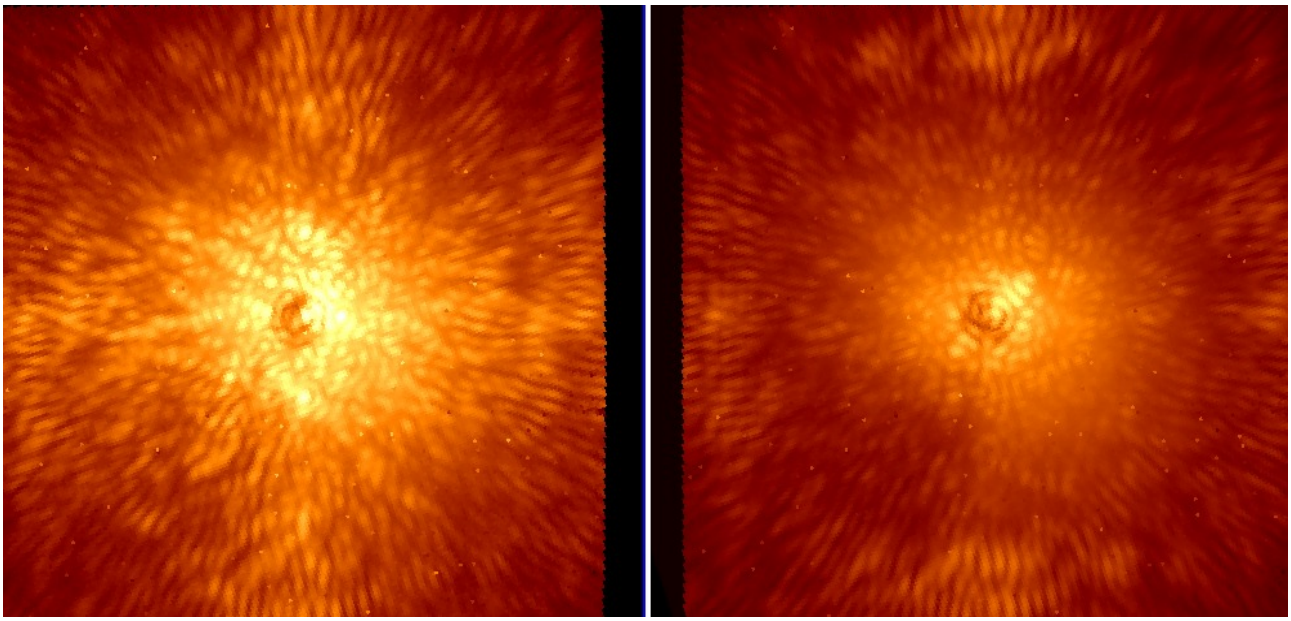

Figure 3: Before and after P1640 coronagraphic images, showing slices of an IFS data cube taken, without and with P-mode control. The square region visible in the right panel is a double-sided dark-hole. The residual speckles seen within the dark-hole are primarily amplitude, while the discernable smooth halo is from the averaged atmospheric leakage.

Atmospheric residuals average out after a few crossing times (the time it takes for wind to sweep a turbulent clump across the telescope, $\sim D/v_{wind}$) into an easily "subtractable" smooth halo (seen in Figure 4 right panel); in a perfect instrument, shot noise from this halo sets the fundamental noise floor in the science image. In a real instrument, however, quasi-static speckles due to slowly varying wavefront aberrations present in the optical train dominate the ability to detect faint companions. Three kinds of aberrations escape the AO control process:

1. The optics located after the AO wavefront sensor / science camera split remain unsensed by the former, so that all the phase and amplitude aberrations present in this portion of the optical train are not corrected at all.
2. AO systems only deal with phase errors measured in the pupil plane, so propagation effects such as the Talbot effect (phase-to-amplitude conversions due to out-of-plane optics) lead to amplitude errors and are not sensed at all.
3. Frequency-folding of phase errors (Give'on et al 2004), appearing within the deformable mirror (DM) control bandwidth, is another Achilles heel of Shack-Hartmann type pupil-plane wavefront sensors. Cross modulation between high spatial-frequency phase terms generates beat spatial frequencies that appear as amplitude speckles within the DM corrected dark hole, setting a hard limit on achievable contrast. Large mirrors, such as primary mirrors of telescopes, have a potential for this kind of problem. Old Shack-Hartmann photographic scans of the Palomar primary mirror reveal that polishing errors on mirror could contribute ~few 10^{-6} amplitude speckles throughout the P1640 focal plane.

Such errors comprise the full suite of non-common path, quasi-static errors that are present downstream at the coronagraph. For example in P1640, the starting non-common-path phase at any new telescope pointing is ~100 nm rms of lower-order modes (0-2 lambda/D) and ~25-30 nm of higher-order modes (2-35 lambda/D).

2.1 Compensating for the quasi-static phase only (P-mode)

Controlling just phase is straightforward. The largest quasi-static errors are phase (typically ~100 nm rms), and amplitude is significantly smaller in comparison. Sensing and correcting phase only provides an immediate jump in contrast performance. When observing bright stars in good seeing conditions, Project 1640 uses all three of its coronagraphic sensors (i.e. tilt, low-order, and high-order wavefront sensors) to continuously measure and track out the quasi-static phase; it does this by sending corrective offset wavefronts to the Palm 3000 WFS, which it turn commands the tweeter-woofer pair of deformable mirrors. When phase are properly addressed we generally find that P1640's contrast floor reaches a limit dominated by amplitude speckles.

All of our survey observing is conducted with phase-only or *P-mode* control. P-mode mirrors conventional adaptive optics, is relatively straightforward to implement and provides major gains for the discovery of companions in broadband light. The P-mode commands a fully symmetric image-plane dark-hole (Fig 3), so that planets may be found anywhere within the instrument's field-of-view. The contrasts achievable in P-mode along with the system's light-gathering capability, determines the number of faint companions P1640 will find in our survey

Some fraction of these P1640's candidate companions may be bona-fide planets, while others will be brown-dwarfs, or unrelated background sources and so a first step is to confirm companionship by acquiring further epochs of data to search for common proper motion with the host star. The next step will be to characterize these objects via low-resolution spectroscopy of the most interesting bound companions (the IFU provides this capability). However, genuine planetary mass companions will be amongst the faintest and only revealed in P-mode images after aggressive speckle post-processing (via IFS's color differential imaging capabilities; Crepp et al. 2011; Pueyo et al. 2012; Oppenheimer et al. 2013; Soummer et al. 2012; Fergus et al. 2014). This post-processing is not lossless. It removes companion flux, generally chromatically, which biases the spectra and can bias the astrometry through distortions. Furthermore, there is the speckle-noise from the remaining speckles. Increasing exposure times to counteract this correlated noise is generally not an option in high contrast imaging.

2.2 Compensating for quasi-static amplitude and phase (E-mode)

As the most interesting companions will almost always lie at the faint end of the instrument's broadband capabilities, obtaining spectroscopy will require further improvement to the operating contrast.

A way around P-mode's limitations is to measure and conjugate the full electric field. This is the basis of P1640's E-mode.
In the most general case phases and amplitudes are fully addressed by adjusting the surfaces of two properly located deformable mirrors (one DM has to be located out-of-plane). But even with a single DM, single-sided dark-holes may be carved in up to one-half of the controllable image (e.g. Malbet, Yu & Shao 1995). When the location of the object is known, a single-sided dark-hole is sufficient for follow-up.

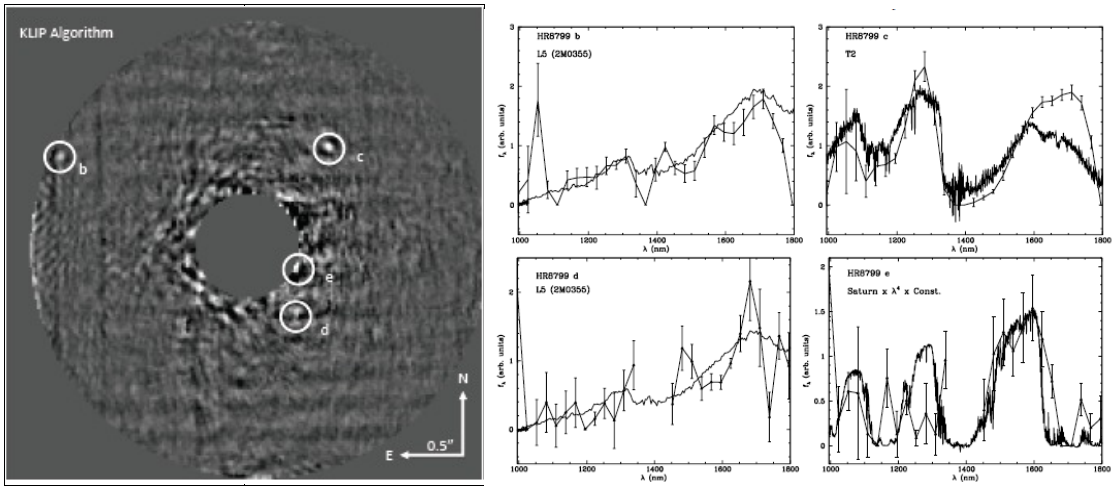

Figure 4: A post-processed P1640 IFS image of the HR 8799 planetary system, taken in June 2012 in P-mode CWFC and post-processed using a principal components analysis algorithm (KLIP; Soummer et al. 2012), along with simultaneously acquired infrared spectra of the four planets HR 8799 b and c (right – top) and d and e (right – bottom). Spectra of the inner planets have lower SNR, because contrasts are worse at small angles, and color differential post-processing is less effective (Oppenheimer et al. 2013). E-mode can overcome these limitations.

Project 1640's wavefront controllers enable in-situ E-field control when conducting science observations. Our interferometric wavefront sensor, which measures the E-field's distortions, can command localized dark-holes with pre-calculated geometries at-and-around a companion's position. Half-plane dark-holes formation is the best we can do given that we have only pupil-plane DMs at our disposal, but this is sufficient when a companion's existence is known. Raw contrasts 2-3 magnitudes deeper than the surrounding image can be obtained in this manner, greatly improving the quality of the science data. The contrasts we have been able to generate within these single-sided dark-holes are the best ever achieved in AO coronagraphy.

3. BRIEF DESCRIPTION OF THE INSTRUMENTATION

Project 1640 and Palm 3000 are discussed in detail in Hinkley et al. (2011) and Dekany et al. (2013). Herein, we provide a quick overview, sufficient to set the stage for the discussion of the wavefront control schemes.

The Hale telescope+Palm 3000+P1640 is a large optical system with 22 optical surfaces before starlight hits the coronagraphic mask; post-mask, there are a further four bounces prior to the suppressed starlight and the surround field-of-view being imaged onto the IFS lenslets.

Palm 3000 has 11 of these surfaces, including a pair of deformable mirrors placed in a tweeter-woofer configuration. The higher-order deformable mirror (HODM) is the largest format deformable mirror to-date with 66x66 actuators behind a continuous face sheet. The lower order deformable mirror (LODM) has 349 actuators.

Palm 3000 delivers ~120 nm rms residual atmospheric correction. Engineering work is on-going to improve the performance to below 100 nm rms, when operating with $V \leq 7$ natural guide stars in median seeing conditions. H-band light, at a wavelength of 1.65 microns, is corrected to ~80-85% Strehl ratio, so that the contribution to planet detection noise from scattered starlight are suppressed by a factor 10^2 compared to seeing-limited observations.

Within P1640 starlight diffraction is suppressed using an apodized Lyot coronagraph (Soummer 2005; Soummer et al. 2011), with a pupil plane apodization providing improvements over a classical Lyot coronagraph and is optimized for operation in the J and H bands. Starlight is rejected at a super-polished, reflective focal plane mask of radius 0.26 arcseconds. The unocculted portion of the image is reflected onto an undersized Lyot stop and then reimaged onto the IFS lenslets. The IFS spectral-camera has a Teledyne H2RG 2k x 2k NIR detector accommodating a 3.8×3.8 arcsec FOV

with 40,000 image samplings which leaves detector real-estate for simultaneous R ~ 30 YJH band low-resolution spectroscopy at all of the image samplings.

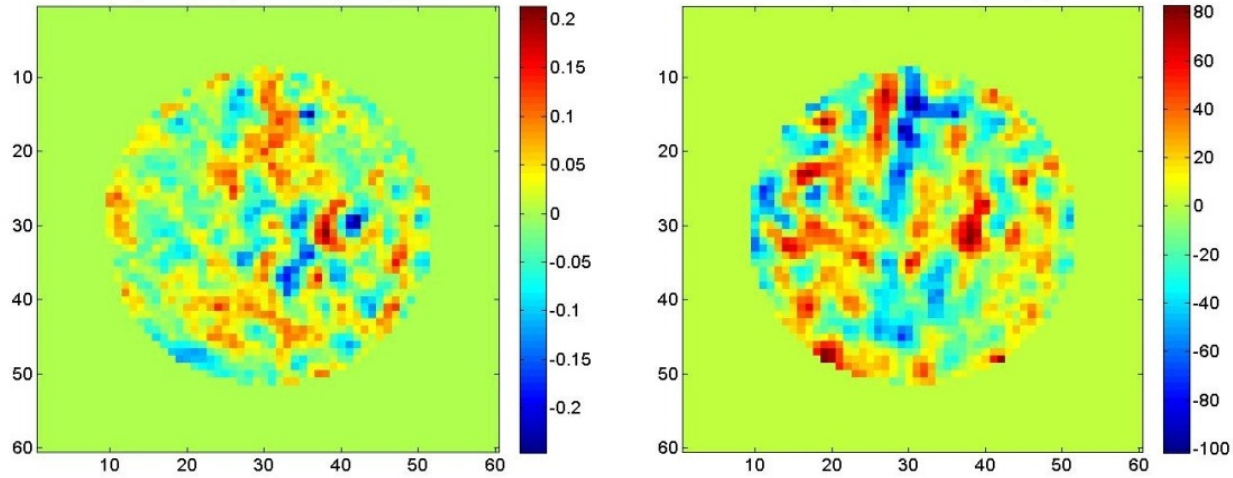

Figure 5: Example quasi-static wavefront measured by CAL in a 100 s integration. The amplitude map (left) has ~4.5 % rms error. The phase map (right) has ~25 nm rms. Such maps are ported to Palm 3000 as centroid offsets, changing the mean DM shape, and controlling the downstream wavefront in the coronagraph.

When Palm 3000 is not on the telescope, the entire instrument can be assembled and used with a pseudo star in the ~400 square foot Palomar AO Laboratory. The AO laboratory is outfitted for engineering development, with extensive optical and electronics equipment for alignment, testing, and validation. For much of this CWFC development, we have used the AO laboratory extensively.

3.1 The Wavefront Calibration System and the CAL wavefront sensor

Project 1640's Wavefront Calibration System is still unique amongst high contrast imagers, and includes three sensors located within the coronagraph: a tip-tilt sensor, a lower-order wavefront sensor and a higher-order wavefront sensor. The higher-order sensor (CAL), an interferometric wavefront sensor, is the only one of relevance here. CAL operates at H-band (the band for which P1640 is optimized), and by virtue of its interferometric design, senses the full pupil plane E-field.

CAL generates quasi-static amplitude and phase maps at ~100 s cadence. In short duration maps, it observes the full

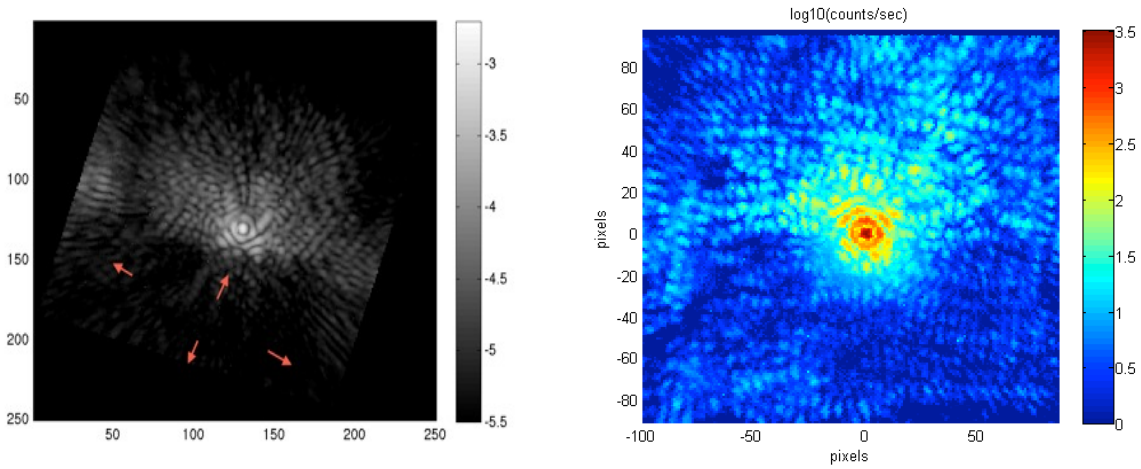

Figure 6: Half plane dark-holes seen at the 1.7um IFS slice of a 6-28λ/D dark hole, created with the PALM 3000 white. The lower half plane is suppressed relative to the P-mode image by ~5. Since total intensity is conserved, the upper half plane gets brighter by ~4. There are Type I E-mode full-half-plane dark-holes.

brunt of the adaptive optics phase residual of ~120 nm rms. However, in 100 s exposures this phase has averaged away to ~2-4 nm rms, at which point the underlying quasi-static structure is revealed to ~5 nm rms accuracy. This averaging property of the AO atmospheric residuals is plotted in Figure 9.

When operating in the standard P-mode, we simply throw away the amplitude maps, retaining and applying only the phase maps to Palm 3000. This is achieved by adjusting the centroid offsets of the AO wavefront-sensor, which in turn commands the two deformable mirrors. In this manner, P-mode controls quasi-static phase to few nanometer levels on sky. In the IFS image-plane conjures a symmetric dark-hole 32λ/D across (figure 4, panel 2). E-mode is an extension of this basic model, except that we will retain the amplitude information. At this stage, we distinguish between Types I and II E-mode. Both will be inplemented as part of this work

3.2 The Type I E-mode

Once P-mode removes bulk quasi-static phases the system's raw contrast ratio is limited by amplitude speckle at ~8×10^{-6} (figure 11). Type 1 E-mode simply uses both amplitude and phase maps to generate DM corrections. As both the HODM and LODM are located at or near a pupil plane, only a single-sided dark-hole is possible here.

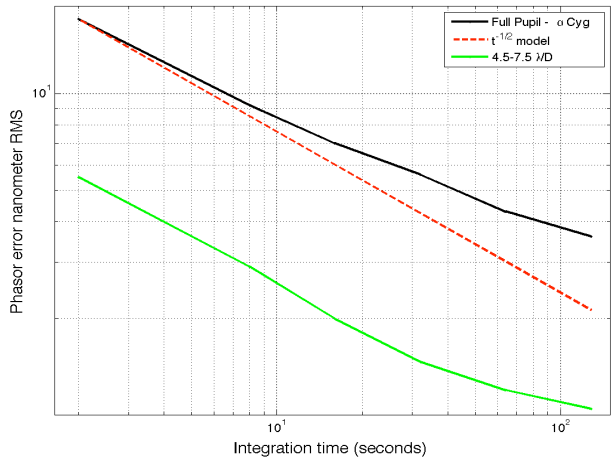

Figure 7: This Allan deviation plot depicts how errors average with time during a CAL measurement of the quasi-static wavefront (see wavefront in Figure 8). Atmospheric AO residual is the largest source of error ~80 nm rms at 0.1 sec timescales (~20 nm at 1 sec). Accordingly, in 100 s integrations, its contribution to final rms error in complex wavefront would be 2 nm rms (in red). Herein, we observe here a leveling of the errors at around 3-4 nm rms (in black), due to temporal "evolution" of the static wavefront. Higher spatial frequency errors (green curve) also evolve somewhat,

A preceding P-mode correction is the starting point for E-mode iterations. A dark-hole region of interest, to null speckles within, is chosen beforehand. The CAL complex maps are fourier transform to generate pseudo-images, thereby providing up-to-date estimates of image-plane E-field, and allowing retrieval of the field at each mode within the specified dark-hole region.

E-mode simultaneously targets all spatial modes in the region of interest. For each mode the pseudo-image provides E-field phasor. Each phasor is used to calculate the exact (sinusoidal) deformable mirror ripple needed to null that phasor. The sum of all sinusoids over all relevant spatial modes, co-added together, estimates the surface deformation needed to null the region of interest. This basic sequence proceeds in an iterative closed loop manner.

The scheme described is similar to a technique called speckle-nulling (Borde & Traub 2006); the primary difference is that we are nulling using CAL's E-field measurements. Since CAL is an offset sensor, this allows us continuously null while carrying on with science exposures. Type 1 E-mode provides a factor of 5 gains in contrast over the basic P-mode (figure 11); this is already a significant forward step for faint companion spectroscopy (E-mode images in figure 8). Next we discuss Type II E-mode, which is more involved, but can potential provide a gain of 10-20.

3.3 The Type II E-mode

Type 1 E-mode rids the image of upstream amplitude and phase speckles. At this stage the remaining specular structure in the image is dominated by errors resulting from the post-coronagraphic non-common path between CAL and the science camera (i.e. IFS), as they are separate instruments.

This is inevitable as the coronagraph is imperfect in its rejection of starlight diffraction. For P1640's APLC, approximately 6% of the field amplitude (4×10^{-3} by intensity) leaks through creating a muted Airy spot at the image

plane. This leaked diffraction accumulates wavefront error from the post-coronagraph optical surfaces forming pinned and other second order specular structure in the image. These non-common path speckles appear at ~1x10^{-6} contrasts.
This speckle floor is addressable via a scheme, which first calibrates the non-common path wavefront error between CAL and the IFS. The fundamental approach is to first create a dark-hole employing the IFS itself as a focal-plane wavefront sensor.
In general, speckle-noise from the dynamic atmospheric errors limits the applicability of direct focal-plane sensing. The incessant speckle activity in any location of the image plane, and the longevity of image speckles of a crossing time, means that it can take more than a 1000 crossing times before a 10^{-6} or slightly fainter speckle can be measured in a "diversity" image, making the entire process prohibitively long. Instead, we adopt a bootstrapping scheme for this Type II E-mode: *generation of the dark-hole in the P1640 science IFS with an artificial , followed by maintenance of the dark-hole during science measurements with CAL.*

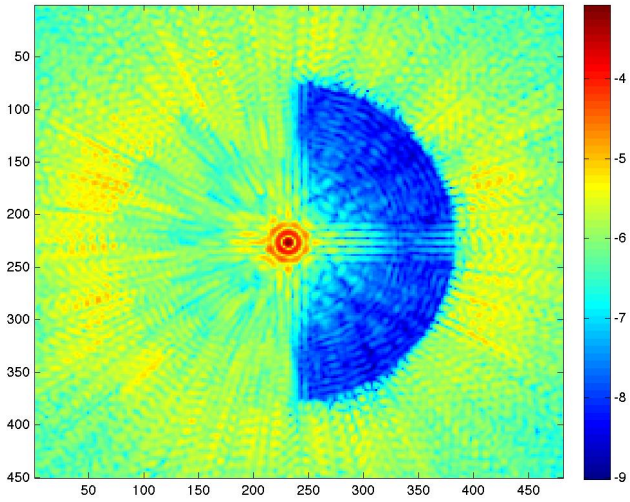

Figure 8: Simulated half plane dark-hole generation using the Palomar Telescope + AO + Project 1640 model prescription, using only 3 full iterations. No atmosphere is included here, so this mimics internal dark-hole generation in Type II E-mode (section 1.2.2). Electric field measurements in 5 sub-bands within H

To generate the dark-hole initially, we use the Electric Field Conjugation algorithm (EFC; Give'on et al. 2006, 2007), which models the effect of poking each actuator in the DM on the dark-hole electric field, $\underline{E}$, and stores the resulting electric fields in a matrix $\underline{G}$. The algorithm then attempts to iteratively find some set of actuator commands $\underline{a}$ such that the difference $\underline{E}+\underline{G}\underline{a}$ is minimized in a least square sense over the dark-hole. This simple formulation can be extended to allow for dark-hole creation at multiple wavelengths, compensate for unmodeled effects in the system, and weight regions of the image plane to greater or lesser extents; see Give'on 2009 for a more extensive treatment. While this algorithm has been implemented using CAL data previously—as, for example, in Figure 8—the CAL camera is filtered to only produce a single H-band image, which is not sufficient to create a dark hole which is maintained across the entire science band accessible to the IFS. Moreover, the Lyot stop is not common-path with the CAL system, and the misalignment between the stop and the model tends to introduce uncorrectable stripes across the dark hole.
Because the IFS is an imaging spectrograph, "deformable mirror diversity" needs to be injected to measure the complex wavefront in its image-plane. A series of shapes or "probes" will be imposed on the PALM 3000 HODM, and the modulated intensities measured as color data-cubes. These data-cubes are demodulated (by color) to derive the image-plane amplitude and phase aberration maps. A transfer function of the HODM-to-IFS optical train, calculated with a Fresnel propagator, is also needed. This and the (color-dependent) aberration maps are used jointly to calculate the HODM actuator offsets needed to cancel the detected field to one side of the image. (As we will use a single deformable mirror, this is a maximum of one-half of the total controllable image; see *e.g.,* Malbet, Yu & Shao 1995).
This entire procedure will be performed using a broadband fiber-fed point source located upstream of the AO system rather than on-sky, although with the telescope boresighted towards the target star to capture pointing-induced flexure. The dark-hole generation must be completed in ≤ 20 min, before the start of hour-long science exposures. During long exposures the residual atmosphere averages to a halo with a noise limits at or below the targeted contrast noise of 10^{-7}. We require the noise from instrumental errors within the dark hole to be at a similar level, and we expect to reach a single sided dark-hole of ~5×10^{-8} in 3–4 iterations. (Thomas et al. 2010) have experimentally demonstrated this level of dark-hole generation for an APLC in their open-air, tabletop, laboratory experiment within a few EFC iterations.) Figure 12 shows the performance of the algorithm for five wavelengths in H-band in our end-to-end Palomar+ Palm 3000+P1640 Fresnel propagation model, which includes representative aberrations on all optical surfaces.

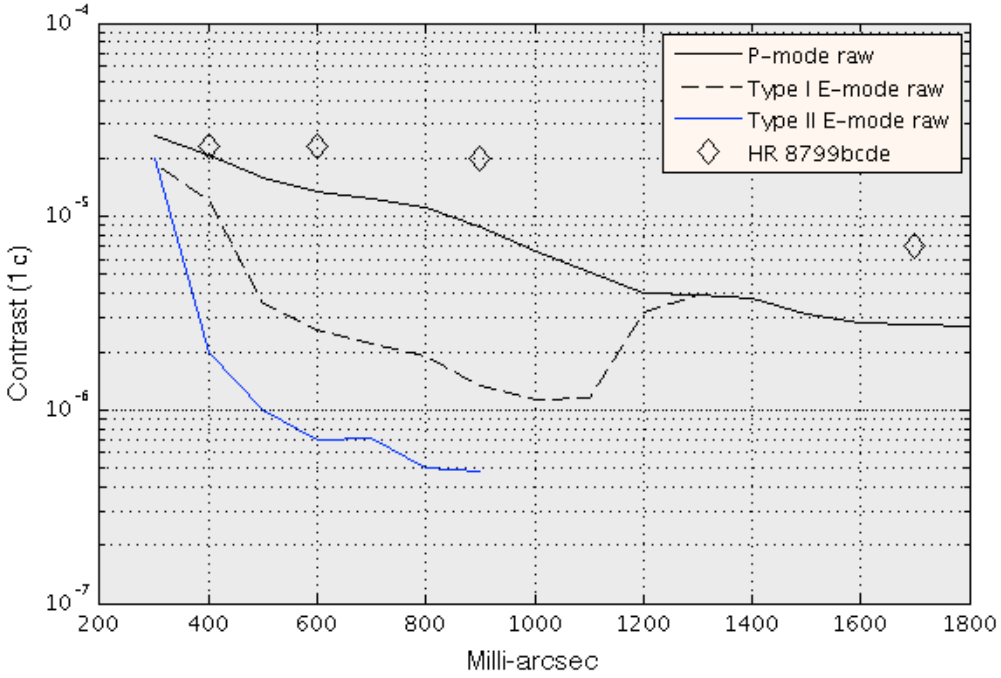

Figure 9: 1-sigma contrast curves for various modes. The Type-I E-mode contrast ratio is measured from actual 0.3-1.0 arcsec single-sided dark-holes. The Type II E-mode contrast curve is a projection based on the analysis of CAL wavefront residuals. All contrasts are for a single 50 nm wide H-band channel. The HR 8799 planets are plotted for reference.

Once the dark hole is in place and stable on the IFS, the wavefront in CAL (W_t) is recorded; this wavefront encodes *all non-common path errors* between CAL and IFS. CAL must now command the HODM back to the target wavefront W_t, rather than its null wavefront; this will maintain the dark hole in the image plane provided that the non-common path errors evolve on a timescale significantly longer than the observation. Both from the design of physically small, and optically tightly integrated optical paths (between the IFS and CAL), and from experience at the telescope, we know that there is almost no perceptible change in the non-common-path between IFS and CAL over large sky angles.
With the dark-hole generated and W_t recorded, the artificial star is removed, the targeted star is rapidly acquired (~1 min), and the AO loops are closed. The inclusion of the upstream optical train, including the primary and secondary, will immediately corrupt the wavefront and the image plane dark-hole in the IFS, and so CAL must command the HODM to bring the difference between the new wavefront W_s and the target wavefront W_t to zero. Throughout the science exposure, CAL will continue to track to W_t rather than the null-wavefront, which will maintain the suppression of quasi-static speckles in the in image plane at the level of a few times 10^{-7} across the dark hole.

This scheme only works well with pupil plane sensor like CAL, which provides significant immunity against the wavefront crossing times, and is highly effective at rejecting atmospheric noise in its measurements.

4. CONCLUSIONS

We have shown that CWFC provides palpable advantages for P1640's overall performance. The basic situation is summarized in figure 11. After slewing the telescope to a new part of the sky before the start of an observation, there is ~30 nm of higher-order phase (along with ~100 nm of low-order phase). A series of preparatory iterations, while observing the artificial star, reduce this to ~5 nm. During an observation this phase can be tracked to ~5-10 nm rms depending on AO performance and stellar magnitude. With this level of phase tracking, the system's contrast is determined entirely by amplitude (which we find to be at a higher than expected level). The limit set by amplitude can be improved using CAL's E-mode setting, which provides both amplitude and phase slope corrections to the Palm 3000

AO, resulting in single sided corrections in the image. The immediate improvement brought about by E-mode control is shown in figure 11 at which stage new limits are set second order non-common-path between the wavefront sensors and the science instrument.

REFERENCES

[1] Baraffe, I., et al, "Evolutionary Models for Cool Brown Dwarfs and Extrasolar Giant Planets. The Case of HD 209458b," A&A, 402, 701 (2003).
[2] Borde', P. J. & Traub, W. A., "High-Contrast Imaging from Space: Speckle Nulling in a Low-Aberration Regime," ApJ, 638, 488 (2006).
[3] Cady, E., Baranec, C. et al., "Electric Field Conjugation with the Project 1640 Coronagraph," Proc. SPIE, 8864E, (2013).
[4] Carson, J., "Direct-Imaging Discovery of a Super Jupiter Around the Late B-Type Star Kappa And.," ApJL, 763, L32 (2013).
[5] Crepp, J. W. & Johnson, J. A., "Estimates of the Planet Yield from Ground Based High Contrast Imaging Observations as a Function of Stellar Mass," ApJ, 733, 126 (2011).
[6] Dekany, R., Roberts, J., Burruss, R., et al., "PALM-3000: Exoplanet Adaptive Optics for the 5.0 m Hale Telescope," ApJ, 776, 130 (2013).
[7] Fergus, R., et al., "S4: A Spatial Spectral Model for Speckle Suppression," ApJ, accepted (2014).
[8] Give'on, A.,et al., "High Frequency Folding and Optimal Phase Conjugation for High Contrast Adaptive Optics," Proc SPIE, 5490, 1438G (2004).
[9] Give'on, A., Shaklan, S. & Green, J. J., "High Dynamic Range Imaging in Space: Overview and Wavefront Control," Proc. SPIE, 6288, 9G (2006).
[10] Give'on, A., et al., "Broadband Wavefront Correction Algorithm for High Contrast Imaging Systems," Proc. SPIE, 6691, pp 66910A-66910A-11 (2007).
[11] Give'on, A., "A Unified Formalism for High Contrast Imaging Correction Algorithms," Proc. SPIE, 7440E, 11G (2009).
[12] Hinkley, S., et al."A New High Contrast Imaging Program at Palomar," PASP, 123, 74 (2011).
[13] Johnson, J. A., et al., "Giant Planet Occurrence in the Stellar Mass-Metallicity Plane," PASP, 122, 905 (2010).
[14] Kalas, P., et al. "Optical Images of an Extrasolar Planet 25 Light-Years from Earth," Science, 322, 1345 (2008).
[15] Lagrange, A. M., et al., "A Giant Planet Imaged in the Disk of the Young Star β Pictoris," Science, 329, 57 (2010).
[16] Macintosh, B. A., "The Gemini Planet Imager: First Light," arXiv:1403.7520 (2014).
[17] Malbet, F., Yu, J. W., & Shao, M., "High Dynamic Range Imaging Using a Deformable Mirror for Space Coronagraphy," PASP, 107, 386 (1995).
[18] Marois, C. et al. "Direct Imaging of Multiple Planets Orbiting the Star HR 8799," Science, 322, 1348 (2008).
[19] Marois, C., et al. "Images of a Fourth Planet Orbiting HR 8977," Nature, 468, 1080 (2010).
[20] Oppenheimer, B. R., Beichman, C. A, Brenner, D. et al., "Project 1640: The World's First Coronagraphic Hyperspectral Imager for Comparative Planetary Science," Proc. SPIE, 8447E, 200 (2012).
[21] Pueyo, L.,et al., "Spectral Characterization of Faint Companions with the Project 1640 Integral Field Spectrograph," ApJS, 199, 6 (2012).
[22] Pueyo, L., et al. 2014, "Reconnaissance of the HR 8799 Exosolar System II: Astrometry and Orbital Motion," ApJ, submitted (2014).
[23] Soummer, R., "Apodized Pupil Lyot Coronagraph for Arbitrary Telescope Apertures," ApJ, 618, 161 (2005).
[24] Soummer, R., Pueyo, L., & Larkin, J., "Detection and Characterization of Exoplanets and Disks using Projections on Karhunen-Loeve Eigenimages." ApJL, 755, L28 (2012).
[25] Thalmann, C.,, "Discovery of the Coldest Imaged Companion of a Sun-like Star," ApJ, 707, L123 (2009).
[26] Vasisht, G., et al. "A Post-Coronagraphic Wavefront Sensor for the TMT Planet Formation Imager," Proc. SPIE, 6272, 161 (2006).
[27] Vasisht, G., Cady, E., Zhai, C., et al.,"Coronagraphic Wavefront Control For Exoplanetary Imaging," PASP, submitted (2014).
[28] Zhai, C. et al. "A first order wavefront estimation algorithm for P1640 calibrator," Proc. SPIE 8447, 6W (2012).